

# A migrating epithelial monolayer flows like a Maxwell viscoelastic liquid

by S. Tlili et al.

## Supplementary Material

### CALCULATION OF TRANSPORT AND ROTATION TERMS

Complete transport and rotation terms are calculated according to Eq. 20 of Tlili et al. [37], and used to plot  $\dot{\epsilon}_r$  in Fig. S2c,f. In brief, the complete evolution equation for  $\epsilon_e$  writes:

$$\partial_t \epsilon_e + v \nabla \epsilon_e = \frac{\nabla v + \nabla v^T}{2} - \dot{\epsilon}_r - \frac{\alpha_g I}{2} + \left( \nabla v - \dot{\epsilon}_r - \frac{\alpha_g I}{2} \right) \epsilon_e + \epsilon_e \left( \nabla v^T - \dot{\epsilon}_r - \frac{\alpha_g I}{2} \right)$$

where  $I$  is the unit tensor,  $\alpha_g = \text{Tr}(\nabla v)$ , and for off-diagonal ( $xy$ ) components we use the convention:

- $\vec{v} = [u, v]$ ,
- $\epsilon_e = \begin{bmatrix} e_{xx} & e_{xy} \\ e_{xy} & e_{yy} \end{bmatrix}$ ,
- $\dot{\epsilon}_r = \begin{bmatrix} d_{xx} & d_{xy} \\ d_{xy} & d_{yy} \end{bmatrix}$ ,
- $\nabla v = \begin{bmatrix} u_x & u_y \\ v_x & v_y \end{bmatrix}$ ,
- $\nabla v^T = \begin{bmatrix} u_x & v_x \\ u_y & v_y \end{bmatrix}$ .

Isolating  $\dot{\epsilon}_r$  from the evolution equation, we find that we can compute it according to:

$$\dot{\epsilon}_r = E^{-1}A$$

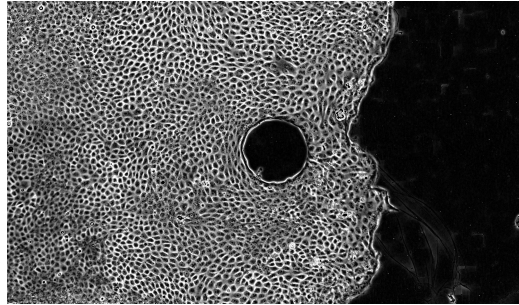
where we define:

- $E = \begin{bmatrix} 1 + 2e_{xx} & 0 & 2e_{xy} \\ 0 & 1 + 2e_{yy} & 2e_{xy} \\ e_{xy} & e_{xy} & 1 + e_{xx} + e_{yy} \end{bmatrix}$ ,
- $A = \begin{bmatrix} A_{xx} \\ A_{yy} \\ A_{xy} \end{bmatrix}$ ,

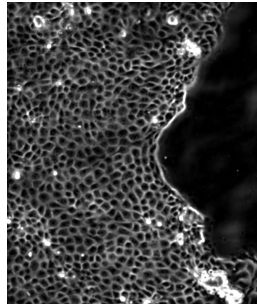
where the components of  $A$  are:

- $A_{xx} = (1 + 2e_{xx})d_{xx} + 2e_{xy}d_{xy}$   
 $= u_x + 2u_x e_{xx} + 2u_y e_{xy} - \alpha_g e_{xx} - \frac{\alpha_g}{2} - (\partial_t e_{xx} + u \partial_x e_{xx} + v \partial_y e_{xx}),$
- $A_{yy} = (1 + 2e_{yy})d_{yy} + 2e_{xy}d_{xy}$   
 $= v_y + 2v_y e_{yy} + 2v_x e_{xy} - \alpha_g e_{yy} - \frac{\alpha_g}{2} - (\partial_t e_{yy} + u \partial_x e_{yy} + v \partial_y e_{yy}),$
- $A_{xy} = (1 + e_{xx} + e_{yy})d_{xy} + e_{xy}d_{xx} + e_{xy}d_{yy}$   
 $= \frac{1}{2}(u_y + v_x) + u_x e_{xy} + v_y e_{xy} + u_y e_{yy} + v_x e_{xx} - \alpha_g e_{xy} - (\partial_t e_{xy} + u \partial_x e_{xy} + v \partial_y e_{xy}).$

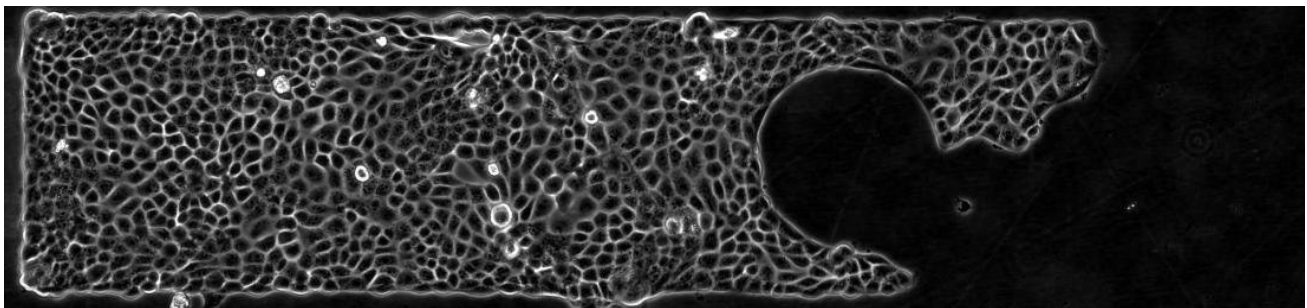
## SUPPLEMENTARY MOVIES



Supplementary Movie 1. Reference experiment, same as Fig. 1; obstacle diameter  $200\ \mu\text{m}$ , strip width  $1000\ \mu\text{m}$ , movie and analysis durations 20 h. Original version: 5 min time interval, pixel size  $0.65\ \mu\text{m}$ ; low-size version: 15 min time interval, pixel size  $2.6\ \mu\text{m}$ .



Supplementary Movie 2. Experiment with myosin activity inhibition, same as Fig. S8a,b; obstacle diameter  $200\ \mu\text{m}$ , strip width  $1000\ \mu\text{m}$ , 5 min time interval, movie duration 12 h, analysis duration 6 h. Original version: pixel size  $0.65\ \mu\text{m}$ ; low-size version: pixel size  $2.6\ \mu\text{m}$ .



Supplementary Movie 3. Experiment without division inhibition, same as Fig. S8c,d; obstacle diameter  $200\ \mu\text{m}$ , strip width  $300\ \mu\text{m}$ , 5 min time interval, movie duration 12 h, analysis duration 4 h. Original version: pixel size  $0.65\ \mu\text{m}$ ; low-size version: pixel size  $2.6\ \mu\text{m}$ .

## SUPPLEMENTARY FIGURES

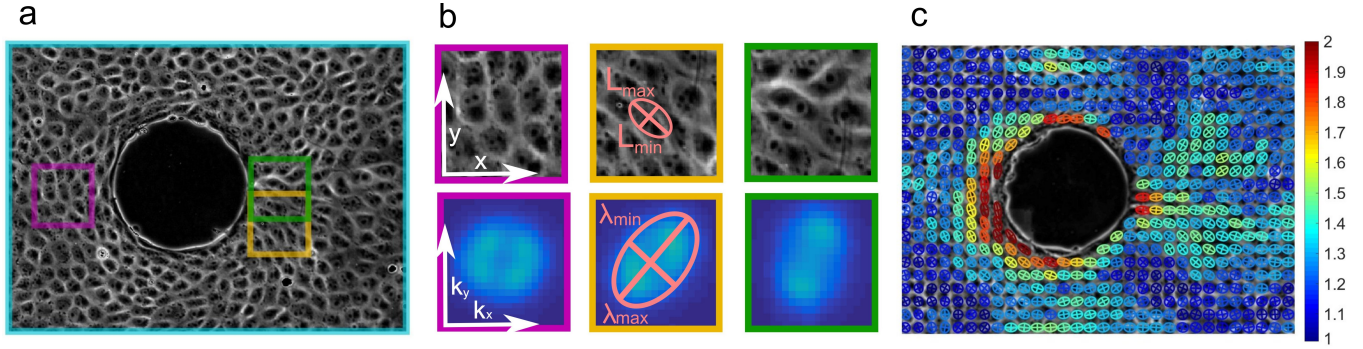


FIG. S1. Fourier Transform. (a) Phase contrast image of the monolayer, same strip as in Fig. 1. (b) 2D Fourier analysis for three different examples of local cell patterns identified in purple, yellow and green boxes in (a). The top panels are in real space and the bottom panels are in Fourier space, with axes indicated in the purple boxes (left). Each Fourier image is blurred using a Gaussian filter and averaged over 8 h. The inertia matrix of the 5% brightest pixels of the image is diagonalized and the pattern is represented as an ellipse (middle, bottom) of axes  $\lambda_{max}$ ,  $\lambda_{min}$ , then their inverses build the ellipse in real space with axes  $L_{max}$ ,  $L_{min}$  (middle, top). (c) Fourier transform map; colors code for the coarse-grained cell anisotropy  $L_{max}/L_{min}$  from 1 (blue) to 2 (red).

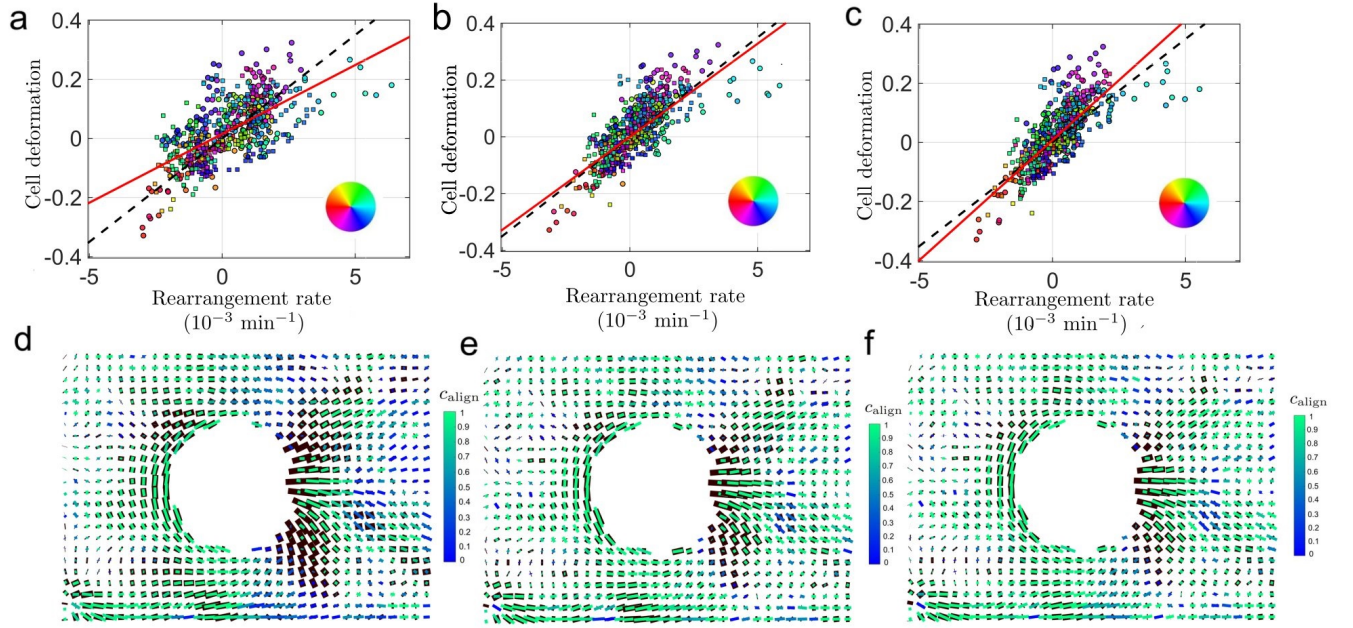


FIG. S2. Coarse-grained cell anisotropy transport and rotation terms. Graphs of  $\varepsilon_e$  vs  $\dot{\varepsilon}_r$  (a – c) and maps of  $\dot{\varepsilon}_r$  (d – f), determined as  $\dot{\varepsilon}_r = \dot{\varepsilon}_{tot} - \dot{\varepsilon}_e = (\nabla v + \nabla v^T)/2 - D\varepsilon_e/Dt$ , using different approximations to estimate  $D\varepsilon_e/Dt$ . (a,d) Neglecting both transport and rotation terms,  $D\varepsilon_e/Dt \approx \partial\varepsilon_e/\partial t$ . (b,e) Taking into account transport but neglecting rotation,  $D\varepsilon_e/Dt \approx \partial\varepsilon_e/\partial t + \vec{v} \cdot \nabla \varepsilon_e$ ; same data as Fig. 3b. (c,f) Complete expression taking into account both transport and rotation (see details in Supplementary Materials and in [37]). Same individual experiment as in Figs. 1, 2; obstacle diameter  $200 \mu\text{m}$ . In graphs (a–c),  $\langle(\varepsilon_e)_{xx} - (\varepsilon_e)_{yy}\rangle/2$  is plotted vs  $\langle(\dot{\varepsilon}_r)_{xx} - (\dot{\varepsilon}_r)_{yy}\rangle/2$  while  $\langle(\varepsilon_e)_{xy}\rangle$  is plotted vs  $\langle(\dot{\varepsilon}_r)_{xy}\rangle$ ; data with  $\varepsilon_e^{\text{dev}}$  amplitude smaller than 0.05 are excluded from the fit. Dashed black lines: slope  $\tau = 70 \text{ min}$ . Solid red lines: linear fit to the data, passing through the origin, slope  $\tau = 47 \text{ min}$  and  $R = 0.62$  for (a),  $\tau = 68 \text{ min}$  and  $R = 0.73$  for (b),  $\tau = 79 \text{ min}$  and  $R = 0.73$  for (c). In each map, same representation as in Fig. 3a, same  $\tau$  value as in the above graph.

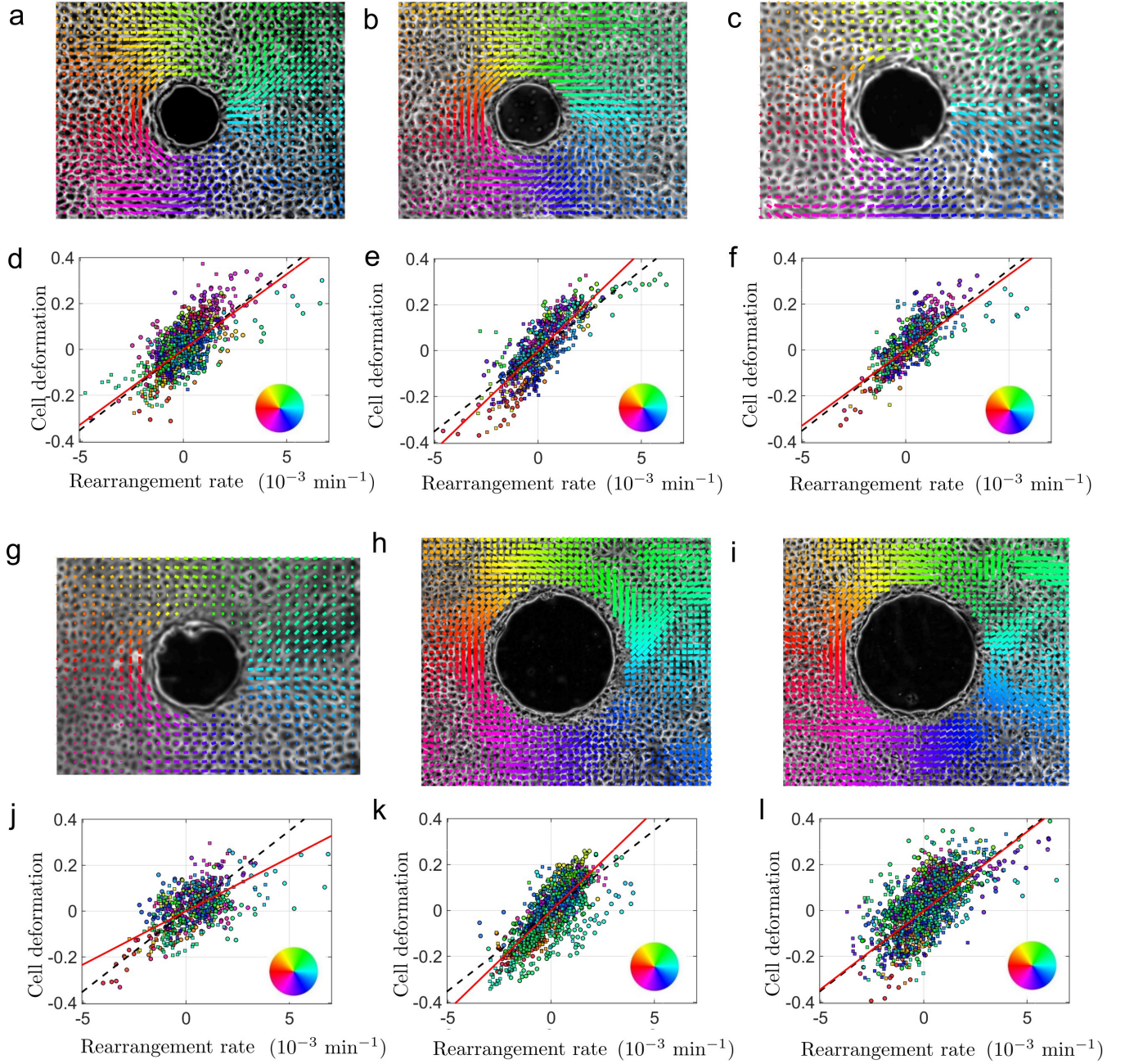


FIG. S3. Determination of viscoelastic time. Three experiment dimensions, each being tested twice for reproducibility: (a, b, d, e) obstacle diameter  $150 \mu\text{m}$ , strip width  $750 \mu\text{m}$ ; (c, f, g, j) obstacle diameter  $200 \mu\text{m}$ , strip width  $1000 \mu\text{m}$ ; (h, i, k, l) obstacle diameter  $300 \mu\text{m}$ , strip width  $1000 \mu\text{m}$ . Top panels (a,b,c,g,h,i): Deviatoric part of the cell deformation tensor; the positive extension axis is represented as a bar. The color codes for the box angle position, in polar coordinate originating at the obstacle center, as in Fig. 2b,c. For legibility, only the cell deformation is represented, not the rearrangement rate. Bottom panels (d,e,f,j,k,l): Cell deformation vs rearrangement rate. Components of the deviatoric tensors are plotted for the six strips, with the same color code as in top panels. Same representations as in Fig. S2. Solid red line: linear fit to the data, passing through the origin; dashed black line: slope 70 min. Note that (f) has the same data as Fig. 3b.  $R$  values: 0.65, 0.78, 0.73, 0.50, 0.76, 0.59.

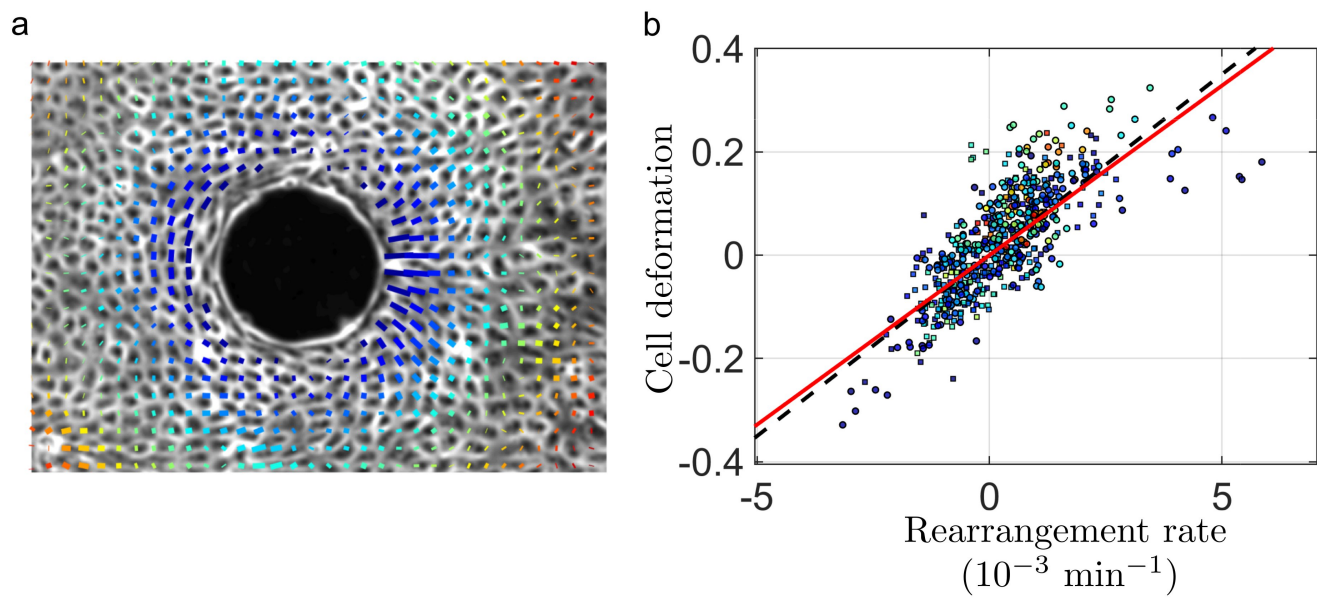


FIG. S4. Range of obstacle effect on flow. Same experiment as in Fig. 3a,b with a different representation. Here, on both panels, the color code of points corresponds to their distance to the obstacle. For legibility, on the left panel only the cell deformation is represented, not the rearrangement rate.

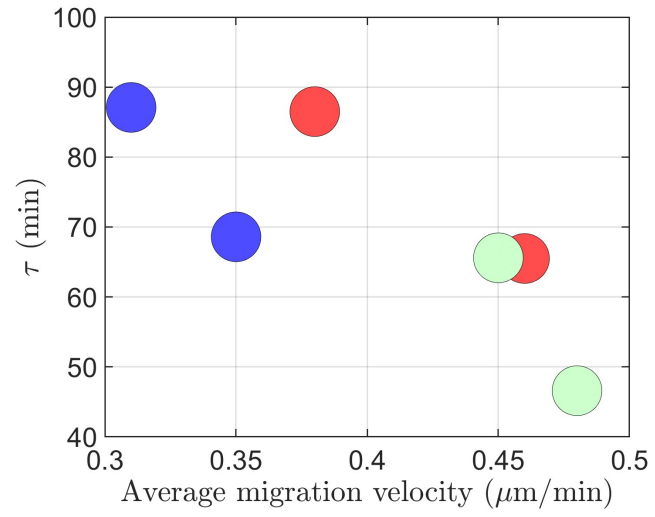


FIG. S5. Viscoelastic time versus monolayer average migration speed, which is the velocity component along  $x$  spatially averaged around the obstacle (on the whole field of view) and temporally averaged during the same duration as the one used for time averaging in the analysis. One point per experiment, same color code as for Fig. 3c.

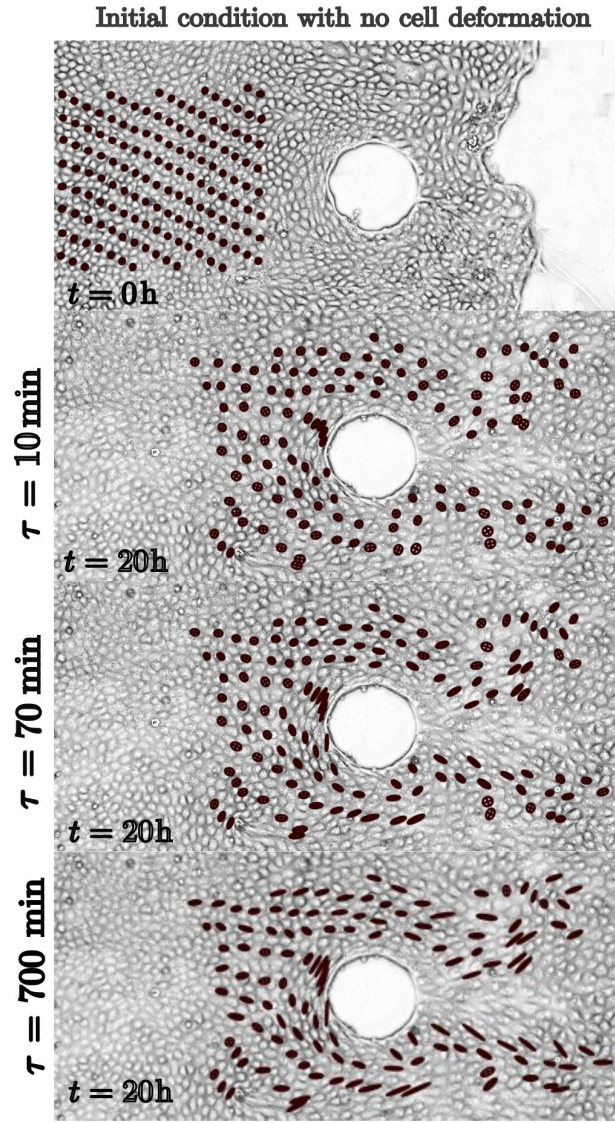


FIG. S6. Visual test of the viscoelastic time value. Assuming the tissue is a viscoelastic liquid with a characteristic time  $\tau$ , we simulate Lagrangian trajectories and deformations of “virtual” cells, which are simply tracers placed on the tissue. (a) Initial condition: 200 tracers placed on a square  $40\ \mu\text{m}$  spaced grid. A tracer labeled  $i$  is assigned a size equal to the actual experimental average cell size in this box, and an initially null deformation  $\varepsilon_e^i(0) = 0$ . The time step is  $dt = 1$  frame  $= 5$  min. At each time-step, the tracer position  $\vec{r}_i(t)$  is advected with its actual experimental velocity field according to  $\vec{r}_i(t + dt) = \vec{r}_i(t) + dt \cdot \vec{v}(\vec{r}_i(t), t)$ . The deviatoric part of its deformation is updated according to a viscoelastic behaviour,  $\varepsilon_e^i(t + dt) = \varepsilon_e^i(t) + dt \cdot ([\nabla v(\vec{r}_i(t), t) + \nabla v^T(\vec{r}_i(t), t)] / 2 - \varepsilon_e^i(t) / \tau)$  while the trace of its deformation is updated according to an elastic behaviour. (b, c, d) Tracer deformation calculated after 24 hours, for three different viscoelastic time values. (b) With  $\tau = 10$  min, the deformation is quickly relaxing as for a pure liquid behavior, and remains much lower than in experiment. (c) With  $\tau = 70$  min, which is the value found in experiments (Fig. 3a,b, Fig. S3), elongations are similar to the experimentally observed elongations, and both elastic and viscous contributions are simultaneously significant. (d) With  $\tau = 700$  min, deformations are much higher than in experiments, as in a pure elastic behavior.

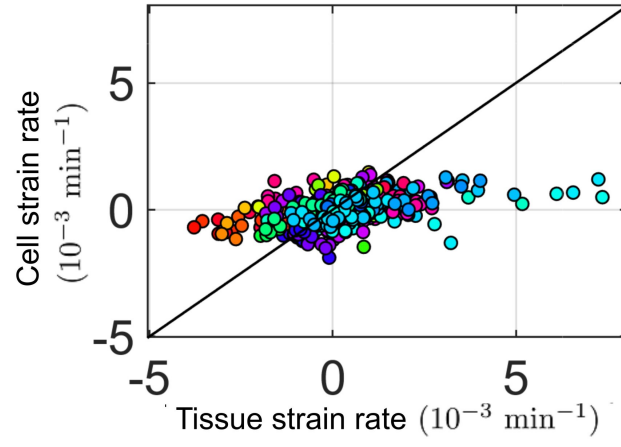


FIG. S7. Rejection of the Kelvin-Voigt model. Plot of the time averaged cellular strain rate  $\langle \frac{\partial \varepsilon_e}{\partial t} + \vec{v} \cdot \nabla \varepsilon_e \rangle$  versus the tissue strain rate  $\langle \nabla v_{\text{sym}} \rangle$ . If the Kelvin-Voigt model, where both quantities are equal, was applicable, all data points would collapse on the first bisectrix (black line).

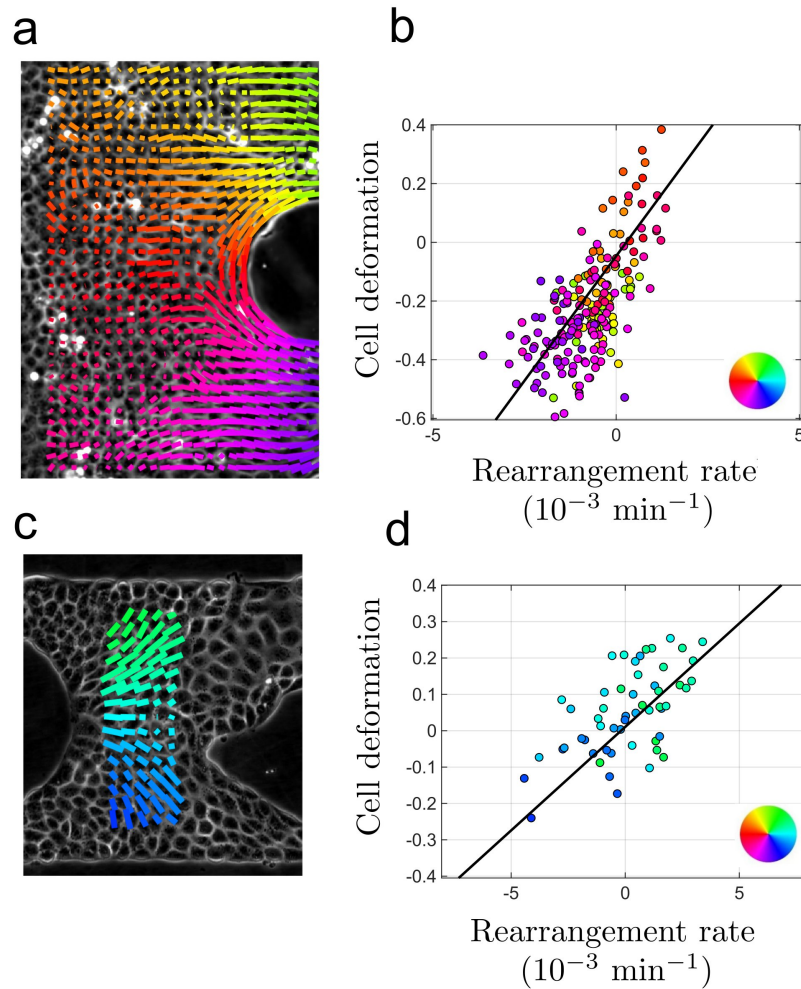


FIG. S8. Effect of drugs on viscoelastic time. (a, b) The myosin activity inhibitor blebbistatin ( $10 \mu\text{M}$ ) is added to the medium at the beginning of the experiment; obstacle diameter  $330 \mu\text{m}$ , strip width  $1000 \mu\text{m}$ . See Supplementary Movie 2. (c, d) Division inhibitor mitomycin is *not* added; obstacle diameter  $200 \mu\text{m}$ , strip width  $300 \mu\text{m}$ . Due to cell density increase and jamming, cells migrate slowly. We analyze the region downstream of the obstacle, where in a few boxes significant cell deformation and migration are consistently observed during a period of 6 hours. See Supplementary Movie 3. In both experiments, since migration is impaired, only part of the boxes display large enough cell deformation and velocity, during a time long enough for averaging purpose, and can be used for the analysis. In the blebbistatin case, steady migration is only observed near the migrating front. In the case without mitomycin, divisions lead rapidly to density increase and tissue jamming at the back of the obstacle.

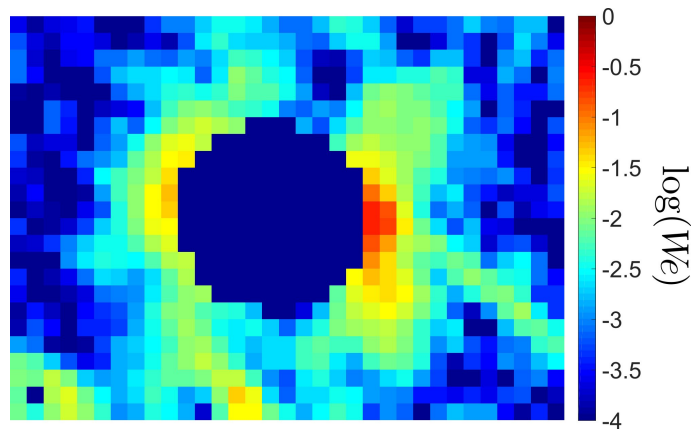


FIG. S9. Weissenberg number map. Same experiment and data as in Fig. 3a. One color per box, in decimal logarithm.